Design and Performance Comparisons of Brushless Doubly-Fed Generators with Different Rotor Structures

Fengge Zhang, *Member*, *IEEE*, Siyang Yu, Yutao Wang, Shi Jin, *Member*, *IEEE*, and Milutin G. Jovanovic, *Senior Member*, *IEEE*

***Abstract*—The Brushless Doubly-Fed Generator (BDFG) shows the great potential for use in large variable speed wind turbines due to its high reliability and cost benefits of a partially-rated power electronics converter. However, it suffers from the compromised efficiency and power factor in comparison with conventional doubly fed induction or synchronous generators. Therefore, optimizing the BDFG, especially the rotor, is necessary for enhancing its torque density and market competitiveness. In this paper, a novel cage-assisted magnetic barrier rotor, called the hybrid rotor, is proposed and analyzed. The detailed analytical design approaches based on the magnetic field modulation theory are investigated. In addition, the machine losses and mutual inductance values using the proposed rotor designs are calculated and their performance implications evaluated. Finally, the comparative experimental results for two BDFG prototypes are presented to verify the accuracy and effectiveness of the theoretical studies.**

***Index Terms*—Brushless doubly-fed generator, hybrid rotor, magnetic field modulation, design principles.**

I. Introduction

DOUBLY-FED machines (DFMs) featuring two AC electrical ports and one mechanical port are widely adopted for renewable energy conversion and variable speed drive systems [1]-[4]. The traditional wound rotor doubly-fed induction machine (DFIM) has been a well-established and proven technology in such applications largely owing to the good overall performance and approximately 30% rated converter over a typical 2:1 speed range. However, the operation & maintenance cost is generally high and reliability is low due to the existence of brushes and slip rings. Therefore, the elimination of these vulnerable components has become one of the focal points of the DFMs research. The brushless doubly-fed machines (BDFMs), including the brushless doubly-fed induction machine (BDFIM) and the brushless doubly-fed reluctance machine (BDFRM), have been getting more attention as a prospective and viable solution to the aforementioned well-known DFIM limitations.

The benefits of the brushless doubly-fed generator (BDFG) such as, no brush gear, robust structure, high reliability and virtually maintenance-free operation as well as the requirement for a small capacity power electronics converter similar to DFIM's, make it a suitable and attractive choice for wind turbines [5]-[8]. Another strong reliability advantage over the DFIM is the inherently medium-speed nature of the BDFG allowing the use of a simpler and more compact 2-stage gearbox as opposed to a high-speed 3-stage counterpart of DFIG wind turbines, which is less mechanically robust and prone to failures [9]. As shown in Fig. 1, unlike conventional AC machines, there are two sets of stator windings with different pole numbers and applied frequencies, the grid-connected primary (power) winding and the converter-fed secondary (control) winding. The magnetic coupling between the stator windings is achieved through an appropriately designed rotor of half the total number of the stator poles. The rotor characteristics are therefore crucial for the BDFM operation. The most commonly used rotors can be of cage and/or reluctance type.

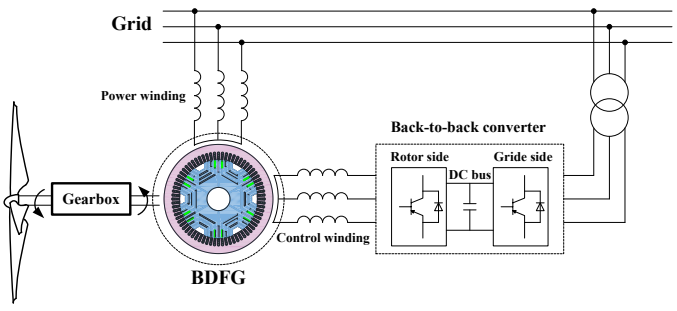

Fig. 1. A conceptual diagram of the wind power BDFG based system.

In order to improve the performance, the rotor construction has always been the focus of the BDFM research. The comparative development and effects of cage and reluctance rotor structures on the BDFM are experimentally investigated in [10]. A generalized torque vector control system for the

Manuscript received October 29, 2017; revised January 28, 2018; accepted February 12, 2018. This work was supported in part by the National Natural Science Foundation of China under Project 51537007. (Corresponding author: Siyang Yu, phone: +86-18842478957, fax: +86-024-25496430, e-mail:yusiyangnuli@163.com.)

Fengge Zhang, Siyang Yu, Yutao Wang and Shi Jin are with the Shenyang University of Technology, Shenyang 110870, China (e-mail: zhangfg@sut.edu.cn; yusiyangnuli@163.com; wangyt3288@163.com; wby-js@163.com).

Milutin G. Jovanovic is with the Faculty of Engineering and Environment, Department of Mathematics, Physics and Electrical Engineering, Northumbria University Newcastle, Newcastle upon Tyne, NE1 8ST, U.K. (e-mail: milutin.jovanovic@northumbria.ac.uk).

BDFIM with a nested-loop rotor is proposed in [11]. A detailed analytical magnetic field model for the same machine is provided in [12], and the rotor temporal and spatial harmonics caused by the winding distribution and slotting are considered. In [13], a new rotor configuration with serially connected loops is proposed to decrease the spatial harmonic distortion of the BDFIG air-gap magnetic field. In [14], a design optimization method for the rotor magnetic circuit is considered to reduce the size and weight of the BDFM. Similarly, a simplified design procedure based on the electromagnetic-thermal model is described in [15] to improve the BDFM power density.

A proportionally smaller amount of research on the BDFRM design has been reported in the literature to date. The rotor pole optimization to increase the no-load EMF and torque of an axial-flux BDFRM is studied in [16]. In [17], the saturation and ducting effects on the BDFRM rotor coupling properties are examined by the finite element analysis. A systematic initial design method for the BDFRM that can be used as a platform for further upgrades is presented in [18].

In this work, a cage-assisted magnetic barrier rotor, also termed as the hybrid rotor, is proposed and analyzed on the basis of the radial magnetic barrier rotor with an incentive to synthesize the best properties of advanced cage and reluctance rotors into a single rotor design for the BDFG performance improvement. The paper is organized as follows. In Section II, a detailed design procedure based on the magnetic field modulation theory is given. The selection principles of the rotor pole, duct number and assisted cage are investigated. In Section III, the comparative performance analysis of the proposed rotor designs is carried out. In Section IV, the experimental results for two 25 kW prototype BDFGs with the considered rotor structures are presented to verify the theoretical studies. Finally, the conclusions are drawn in Section V.

II. BDFG Design Aspects

A. Background Theory

The BDFM can be operated in a variety of modes, such as asynchronous and synchronous. The BDFM speed (rev/min) can be written as [14]:

$$n_r = 60\left(f_p \pm f_c\right)/p_r \tag{1}$$

where the subscripts p and c denote the power and control windings, respectively, f denotes the winding frequency (Hz), and p_r indicates the rotor pole number. The BDFM essentially behaves as a classical synchronous machine if the control winding is connected to a DC source, operating at so called natural synchronous speed under this condition. Note that the latter is half the synchronous speed of an equivalent DFIG having the same number of rotor poles which implies that a 2-stage, rather than a 3-stage, gearbox can be used for BDFG based wind turbines with immediately obvious reliability and economic benefits [9]. If a positive sequence frequency is applied to the control winding, i.e. "+" in (1), the BDFM is in super-synchronous speed mode. Else, if the control winding has a 'negative' phase sequence (i.e. contrary to the primary winding) corresponding to "-" in (1), the BDFM is operated in sub-synchronous mode. In generating (BDFG) regime, the power winding frequency can be expressed from (1) as:

$$f_p = p_r n_r/60 \pm f_c \tag{2}$$

It can be seen that f_p can be kept constant by regulating f_c for a given rotor speed. Therefore, the BDFG is suitable for variable speed constant frequency (VSCF) generation systems.

The voltage state equation for the BDFG can be written in matrix form using conventional notation as:

$$\boldsymbol{u} = \boldsymbol{R}\boldsymbol{i} + \frac{d}{dt}\left(\boldsymbol{L}\boldsymbol{i}\right) = \left(\boldsymbol{R} + \omega_r \frac{d\boldsymbol{L}}{d\theta_r}\right)\boldsymbol{i} + \boldsymbol{L}\frac{d\boldsymbol{i}}{dt} \tag{3}$$

where $\omega_r = p_r\omega_{rm} = d\theta_r/dt$ denotes the rotor 'electrical' angular velocity. The equation of motion for a lumped-inertia load (J) in standard form is as follows:

$$T_L = T_{em} + J\frac{d\omega_{rm}}{dt} \tag{4}$$

where T_L and T_{em} signify the mechanical torque of the prime mover and the BDFG electromagnetic torque, respectively. Furthermore, T_{em} can be expressed as [10]:

$$T_{em} = \frac{3}{2}p_r L_{prc} i_p i_c \sin\beta \tag{5}$$

where L_{prc} represents the mutual inductance between the power and control windings of the current magnitudes i_p and i_c, respectively, and β is the angle between the induced phase voltage and current.

B. Rotor Design Process

Cage and reluctance rotors used for the BDFG have their own advantages and limitations. While the former is generally easier to manufacture, the latter offers the superior performance but at the expense of manufacturing difficulties, especially in the case of the axially-laminated-anisotropic (ALA) design [19]. In order to combine the advantages of these two rotor types, a clone cage-assisted magnetic barrier rotor, referred to as the hybrid rotor, which integrates the cage and radially laminated reluctance rotor is proposed as shown in Fig. 2.

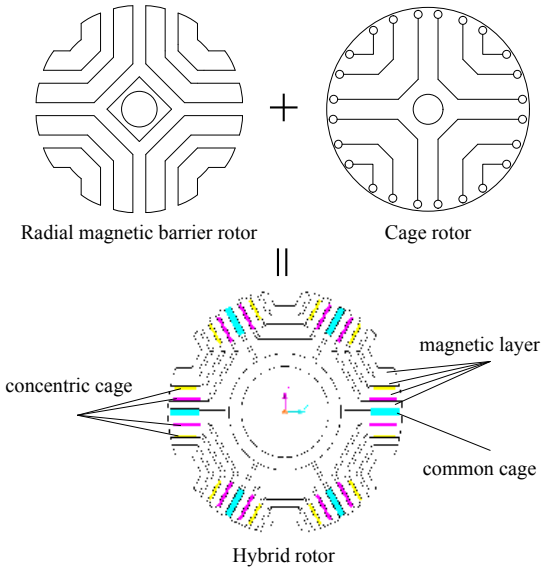

Fig. 2. The hybrid rotor structure.

1) Selection of Rotor Pole Number:

The number of rotor poles of the BDFG is directly related to the pole number of the stator windings, and it can be determined using the magnetic field modulation theory. The air-gap flux density of the BDFG can be written as [20]:

$$B = B_p + B_c \tag{6}$$

$$\begin{aligned} B_p &= \hat{F}_p \lambda_0 \cos\left(p_p\varphi - \omega_p t\right) \\ &+ \hat{F}_p \frac{\lambda_1}{2}\cos\left[\left(p_p + p_r\right)\varphi - \left(\omega_p + p_r\omega_{rm}\right)t - p_r\theta_{r0}\right] \\ &+ \hat{F}_p \frac{\lambda_1}{2}\cos\left[\left(p_p - p_r\right)\varphi - \left(\omega_p - p_r\omega_{rm}\right)t + p_r\theta_{r0}\right] \end{aligned} \tag{7}$$

$$\begin{aligned} B_c &= \hat{F}_c \lambda_0 \cos\left(p_c\varphi - \omega_c t - \gamma\right) \\ &+ \hat{F}_c \frac{\lambda_1}{2}\cos\left[\left(p_c + p_r\right)\varphi - \left(\omega_c + p_r\omega_{rm}\right)t - p_r\theta_{r0} - \gamma\right] \\ &+ \hat{F}_c \frac{\lambda_1}{2}\cos\left[\left(p_c - p_r\right)\varphi - \left(\omega_c - p_r\omega_{rm}\right)t + p_r\theta_{r0} - \gamma\right] \end{aligned} \tag{8}$$

where $\hat{F}$ and ω denote the peak magneto-motive force (MMF) and angular supply frequency of each winding, p_p and p_c indicate the pole-pair number of the power and control windings, respectively, θ_{r0} and φ are mechanical angles referring to the rotor initial position and an arbitrary point on the stator periphery respectively, both with reference to the power winding phase A-axis, whereas γ represents a phase angle of the control winding a-phase current. The average value (λ_0) and the fundamental harmonic amplitude (λ_1) of the air-gap permeance in (7) and (8) can be formulated as follows:

$$\lambda_0 = \alpha_p \frac{\mu_0}{g} \tag{9}$$

$$\lambda_1 = 2\left[\frac{\sin\left(\alpha_p\pi\right)}{\pi}\right]\frac{\mu_0}{g} \tag{10}$$

where α_p denotes the pole-arc factor, μ_0 is the magnetic permeability of vacuum, and g is the air-gap width.

The magnetic coupling between the stator windings occurs if the space and time harmonics of B_p side-band terms in (7) equal the counterparts in the B_c fundamental component of (8), and vice-versa. Hence, in order to achieve the electro-mechanical energy conversion in the machine, the rotor pole number should satisfy the following relationship:

$$p_r = p_p \pm p_c \tag{11}$$

where "+" refers to the "sum modification" mode, and "-" to the "differential modification" mode. In the latter case, the electromagnetic torques coming from the stator windings are in opposite direction i.e. they counter-act implying that the resultant electromagnetic power (P_{em}=$T_{em}\omega_{rm}$) of the BDFG is the difference between the inputs provided by each winding according to (5). On the other hand, the individual contributions of the windings in the P_{em} production add up when the sum modification mode is adopted, which is therefore a preferable choice in terms of the achievable power density of the BDFG.

The odd rotor pole numbers are susceptible to unbalanced magnetic pull [21]. In addition, rotor designs with 4 poles (i.e. a 6/2 stator poles combination) may have unwanted coupling between the windings: any saturation-induced third harmonic of the 2-pole winding will directly couple the 6-pole one. For this reason, the lowest reasonable rotor pole number may be taken to be 6, and such an arrangement with the 8/4-pole stator windings is investigated in this paper.

2) Selection of Rotor Duct Number:

For the magnetic barrier reluctance rotor, the duct can be considered as a single "slot". An inappropriate combination of the slots may lead to torque ripples, undesirable harmonics and audible noise. In order to characterize the slotting effects on the magnetic field modulation, the coupling factor (C_f) is defined by the modulated flux density and primitive MMF as:

$$C_f = \frac{\hat{B}_p}{\frac{\mu_0}{g}\hat{F}_c} = \frac{\hat{B}_p}{\frac{\mu_0}{g}\frac{3\sqrt{2}}{\pi}\frac{N_c k_{N1c}}{p_c}I_c} \tag{12}$$

where N and k_{N1} denote the number of turns per phase and fundamental winding coefficient, respectively, and I indicates the RMS current.

Furthermore, the number of rotor ducts must be an integer multiple of the number of rotor segments. Given the BDFG example considered in this paper, the number of rotor ducts must be an integer multiple of 6, and the number of stator slots must be an integer multiple of 24 providing that the stator slots per pole per phase is an integer. If the latter is 3, the possible combinations are presented in Table I. It can be seen that the C_f value is the highest when the rotor duct number is 42. In other words, for the calculation case, the 6-pole and 42-slot combination can maximize the rotor coupling capacity.

TABLE I
SLOTS COMBINATION OF STATOR AND ROTOR

Slots of stator	Ducts of rotor	B_4 / T	B_8 / T	C_f [%]
72	18	0.5727	0.4573	79.85
	30	0.5752	0.4715	81.96
	42	0.5714	0.4787	83.77
	54	0.5744	0.4764	82.94
	66	0.5657	0.4718	83.39

3) Selection of Assisted Cage:

For the hybrid rotor, the common cage or concentric cage, shown in Fig. 2, can be used. The assisted cages are located in the ducts, so their number depends on the number of rotor ducts. The influence of common cage on the magnetic field modulation can also be established from Table II. Notice that the C_f of the rotor with a common cage is about 20% higher than without it. Thus, the common cage can significantly improve the coupling capacity of the magnetic barrier rotor.

TABLE II
EFFECT OF COMMON CAGE ON COUPLING CAPABILITY

Condition	C_f [%]
With common cage	105.24
No common cage	83.77

This article has been accepted for publication in a future issue of this journal, but has not been fully edited. Content may change prior to final publication. Citation information: DOI 10.1109/TIE.2018.2811379, IEEE Transactions on Industrial Electronics

According to the analysis above and Fig. 3, the maximum group number of concentric cage (GNCC) is 3. Given the results in Fig. 3, the C_f increases with the increasing GNCC but remains more or less the same when GNCC > 2. Therefore, for the prototype analyzed in this paper, the GNCC is selected to be 2 taking the rotor copper loss and manufacturing into account.

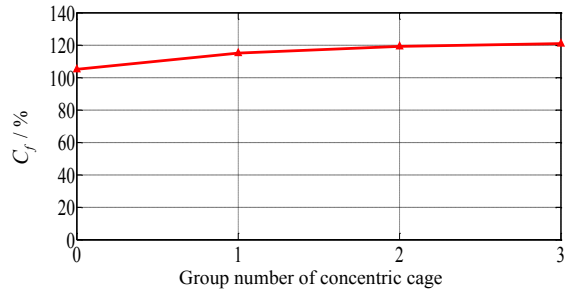

Fig. 3. Effect of concentric cage group number on coupling capability.

C.Hybrid Rotor Analysis

The coupling capacity of the hybrid rotor is investigated using the magnetic field modulation theory. The magnetic field of the BDFG with the magnetic barrier rotor is modulated by the flux guides, which are usually put together to form the flux guide segments consisting of multiple magnetic layers and insulated by non-magnetic materials as shown in Fig. 4. Therefore, each magnetic layer behaves like a flux tube that only allows the flux lines to enter or exit from the two points symmetrical around the middle line of each flux guide segment.

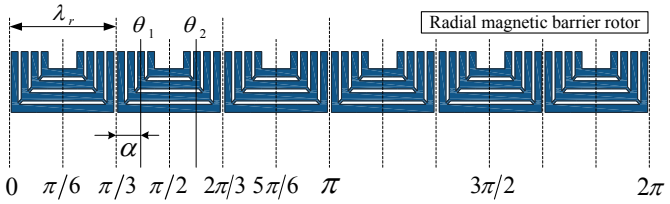

Fig. 4. Expansion diagram of a 6-pole radial magnetic barrier rotor.

The MMF of each phase winding is the product of its current and the winding function (W), which can be expressed as [22]:

$$W(\theta)=n(\theta)-\bar{n}(\theta) \tag{13}$$

where $n(\theta)$ denotes the turns function of average value $\bar{n}(\theta)$ that can be formulated in a usual manner as:

$$\bar{n}(\theta)=\frac{1}{2\pi}\int_0^{2\pi} n(\theta)d\theta \tag{14}$$

By symmetry of the rotor magnetic circuit structure, the fluxes of the two points belonging to the same magnetic circuit loop are equal (e.g. θ_1 and θ_2 in Fig. 4). Therefore, the flux density at θ_1 can be calculated as:

$$B(\theta_1)=\frac{1}{2}\frac{\mu_0}{g}\left[W(\theta_1)\cdot i_e - W(\theta_2)\cdot i_e\right] \tag{15}$$

where i_e is the excitation current. Besides,

$$2k(\lambda_r/2)<\theta_1<(2k+1)(\lambda_r/2) \tag{16}$$

$$\theta_2=\theta_1+\lambda_r-2\alpha \tag{17}$$

$$\lambda_r=2\pi/p_r \tag{18}$$

$$\alpha=\mathrm{mod}(\theta_1,\lambda_r) \tag{19}$$

where k equals the segment order subtract 1, and α indicates the angular distance between θ_1 and the start of the relevant segment as illustrated in Fig. 4.

The air-gap magnetic flux density of each area can be calculated using (15) - (19). The detailed modulation process of the air-gap flux density by the rotor is shown in Fig. 5.

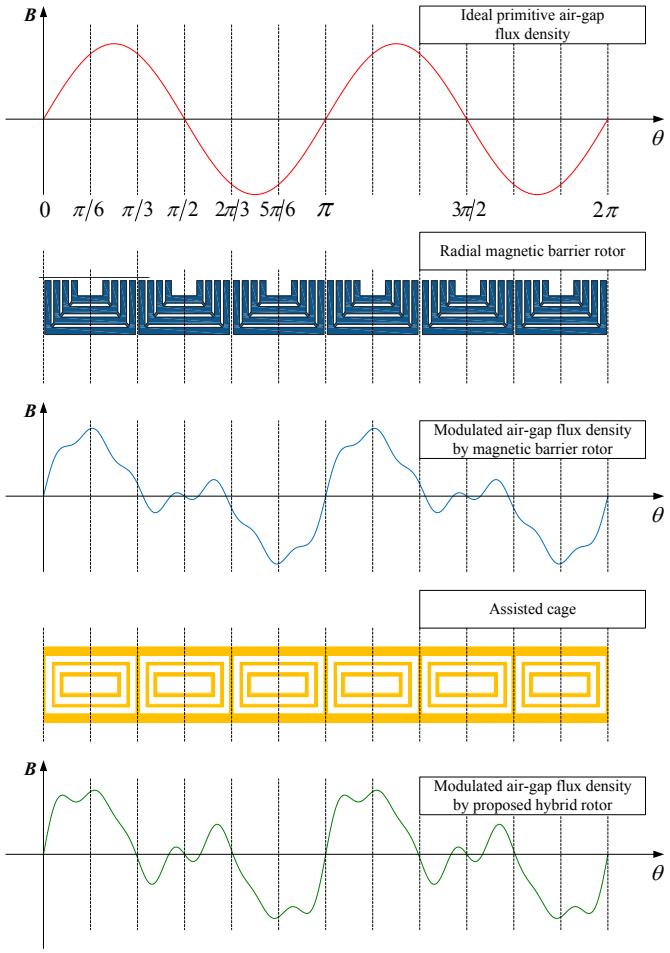

Fig. 5. Modulation of the air gap flux density in the BDFG with the hybrid rotor ($p_p=4$, $p_c=2$, $p_r=6$).

The assisted cages in the hybrid rotor allow the flux to flow along the desired path. Moreover, currents will be induced in the assisted cages, and the respective MMF produced will also impact the air-gap flux density. As a consequence, the harmonics pole pair number of the resultant air-gap flux density modulated by the hybrid rotor contains p_e , $N\cdot p_r$ and $N\cdot p_r \pm p_e$, where p_e represents the pole pair number of the excitation winding and N is an integer. The corresponding harmonic spectrum for the specified operating condition is presented in Fig. 6.

The comparative results of the output voltage THD are presented in Fig. 7. It can be seen that the assisted cages can improve the output voltage waveform and reduce the THD. Furthermore, in the no-load case, the excitation current of the

This article has been accepted for publication in a future issue of this journal, but has not been fully edited. Content may change prior to final publication. Citation information: DOI 10.1109/TIE.2018.2811379, IEEE Transactions on Industrial Electronics

BDFG with the radial magnetic barrier rotor is higher than with the hybrid rotor for the same output voltage. This also means that the magnetic field modulation of the hybrid rotor is better than that of the magnetic barrier counterpart.

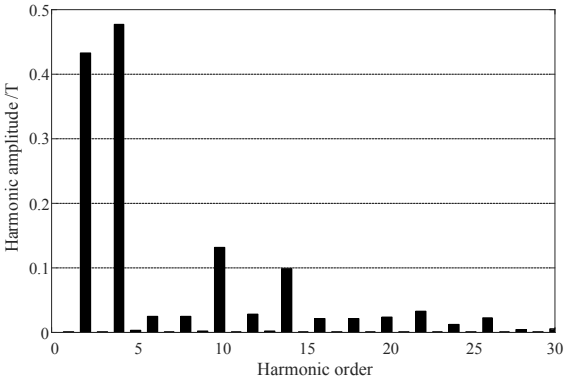

Fig. 6. Harmonic spectrum of the BDFG with the hybrid rotor ($p_e = p_c = 2$).

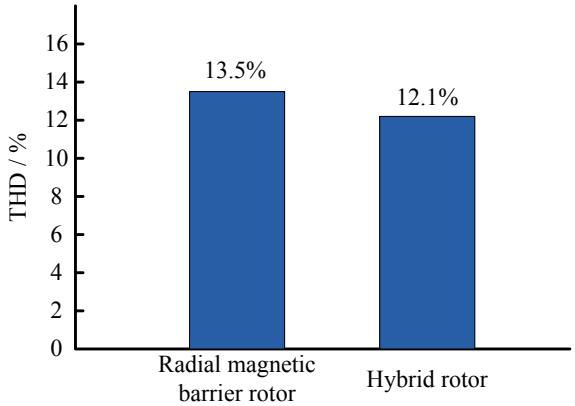

Fig. 7. The output voltage THDs provided by the considered rotor structures.

Although the magnetic field modulation behavior shifts the distribution of magnetic field, the total power content is kept constant no matter what kind of modulation is used [23]. In order to evaluate the modulation efficacy, the modulation factor (M_f) is defined as the ratio of the effective modulated MMF components to total MMF component. i.e.,

$$M_f = \sqrt{\sum_{\nu\in E}|F_\nu|^2 \Big/ \sum|F|^2} = \sqrt{\sum_{\nu\in E}|F_\nu|^2 \Big/ \left(\frac{1}{\mu_0{}^2}\sum\left|\int_0^L B\cdot dl\right|^2\right)} \tag{20}$$

where E is the set of orders of effective components of the modulated MMF, and L denotes the length of magnetic circuit. According to (20), the M_f of the radial magnetic barrier and hybrid rotors shown in Fig. 5 is 0.334 and 0.426, respectively. From the results obtained it can be concluded that the modulation effect of the hybrid rotor is superior to the radial magnetic barrier rotor. In other words, the assisted cage can effectively improve the coupling capacity.

III. Performance Predictions

In order to better describe the BDFG performance with the hybrid rotor, the machine losses and mutual inductance are calculated and analyzed in detail in this section.

A. Loss Calculations

Due to the peculiarity of the structure and complexity of the magnetic field, the calculation of the BDFG losses is much more complex than with traditional generators. For their accurate estimation, both the copper and core loss calculation methods are investigated below.

1) Copper Losses:

The power and control windings of the BDFG with the magnetic barrier rotor are made of random coils with a small wire diameter and negligible skin effect. Therefore, the total copper losses can be calculated directly as:

$$p_{Cu} = p_{CuS} = 3I_p^2R_p + 3I_c^2R_c \tag{21}$$

where R and I denote the resistance and the RMS current, respectively.

However, because of the existence of assisted cages in the hybrid rotor, the rotor copper losses should also be considered in this case. The equivalent circuit of the hybrid rotor cages is shown in Fig. 8.

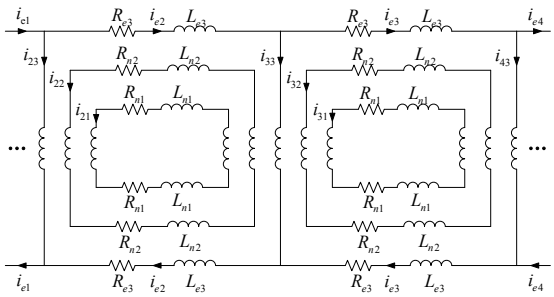

Fig. 8. Equivalent circuit of hybrid rotor cage bars (the subscript *e* and *n* denote the end ring and nested-loop, respectively).

Using Fig. 8, the rotor copper losses can be expressed as:

$$p_{CuR} = \sum_{i=1}^{6}\sum_{j=1}^{2}\left(I_{ij}^2R_j + I_{i3}^2R_{l3} + 2I_{ei}^2R_{e3}\right) \tag{22}$$

where the subscripts i, j, and l denote the nest and loop number of assisted cages, and "linear part", respectively, and:

$$R_j = 2\left(R_{nj} + R_{lj}\right) \tag{23}$$

The end-ring current can be expressed as:

$$i_{ei} = i_{e,i+1} + i_{i+1,3} \tag{24}$$

According to (21)-(24), the total copper losses of the BDFG with the hybrid rotor can now be calculated as:

$$p_{Cu} = p_{CuS} + p_{CuR} \tag{25}$$

2) Core Losses:

Compared with the copper losses, the core loss estimation is even more complicated. It can be seen from Fig. 9 that the BDFG harmonic content is higher than with conventional generators, so the harmonic effects should be accounted for in the core loss assessment.

Furthermore, the magnetic field in the iron core varies both in temporal and spatial terms, so the hysteresis loss, eddy-current loss and additional losses will be produced. In order to analyze the BDFG magnetization, some characteristic points are identified as per Fig. 10. According to Fig. 11, the magnetization properties of each point are different, and most of the points have irregular rotating magnetizing curves.

This article has been accepted for publication in a future issue of this journal, but has not been fully edited. Content may change prior to final publication. Citation information: DOI 10.1109/TIE.2018.2811379, IEEE Transactions on Industrial Electronics

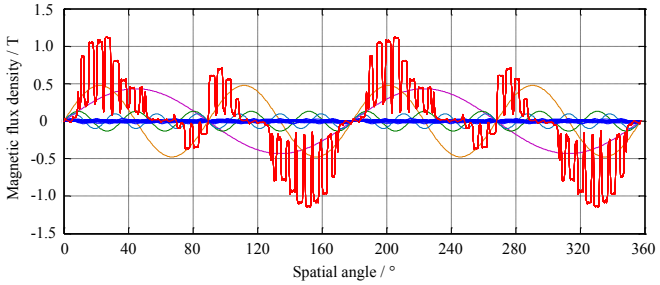

Fig. 9. Composition of the air-gap magnetic flux density.

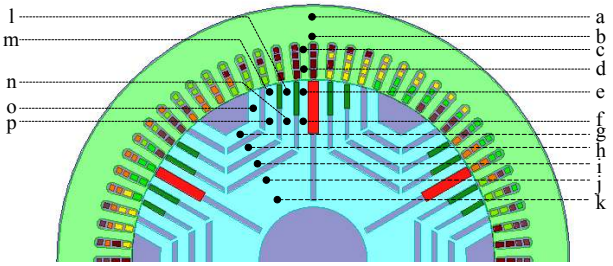

Fig. 10. Magnetic density calculation points of BDFG.

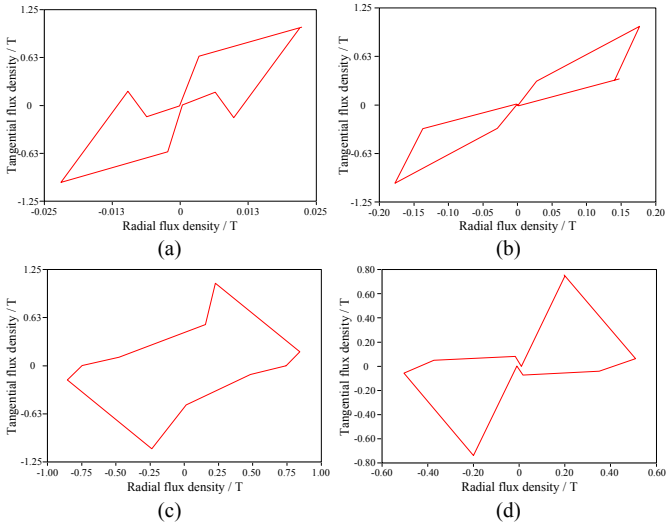

Fig. 11. Magnetization characteristic waveform of different points: (a) c point; (b) o point; (c) n point; (d) i point.

The classical Bertotti loss calculation model [24] only considers the core loss caused by alternating magnetization. Therefore, in order to estimate the core losses accurately, the effects of both alternating and rotating magnetization should be taken into account. The irregular rotating magnetization can be assumed equivalent to a series of elliptical characteristics as illustrated in Fig. 12, and the latter can be considered as two cross alternating magnetizations.

The core loss model including the effects of harmonic flux density, rotating magnetization and alternating magnetization can be represented as follows [25]:

$$p_{Fe} = p_h + p_c + p_e = K_h f \sum_{k=0}^{\infty} k \left(B_{k\max}^{\alpha} + B_{k\min}^{\alpha} \right) + K_c f^2 \sum_{k=0}^{\infty} k^2 \left(B_{k\max}^{2} + B_{k\min}^{2} \right) + \frac{K_e}{(2\pi)^{3/2}} \frac{1}{T} \int_0^T \left(\left| \frac{dB_r(t)}{dt} \right|^{1.5} + \left| \frac{dB_\theta(t)}{dt} \right|^{1.5} \right) dt \quad (26)$$

where K_h, K_c and K_e indicate the coefficient of hysteresis loss, eddy-current loss and added loss, respectively, $B_{k\max}$ and $B_{k\min}$ are the long axis and short axis of k sequence oval harmonic magnetic flux density, respectively, whereas $B_r(t)$ and $B_\theta(t)$ are the radial and tangential components of the magnetic flux density, respectively.

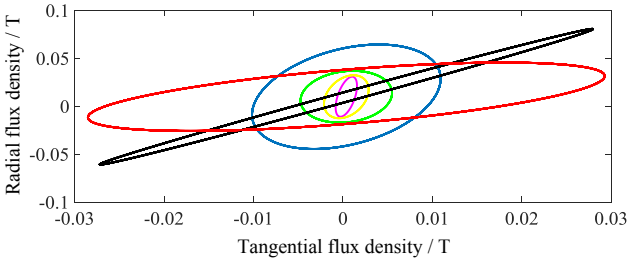

Fig. 12. Elliptical flux density of i point.

B. Mutual Inductance Analysis

The induced voltage required for the electro-mechanical energy conversion in the BDFG is caused by the rotor position dependent variation of the mutual inductance between the stator windings. Therefore, the coupling capacity of the rotor is particularly important for the BDFG performance, and the mutual inductance can be used as an effective measure to properly characterize the degree of such magnetic coupling.

An inductance evaluation method based on the modified winding function is adopted [26]. The superposition principle is used to determine the air-gap permeance function. The mutual inductance calculation results applying the numerical approach proposed in [26] for the 8/4-pole BDFG with the 6-pole hybrid rotor are presented in Fig. 13. The corresponding comparative waveforms for the two rotor types under consideration are shown in Fig. 14. Notice that the mutual inductance offered by the hybrid rotor is higher than that of the radial magnetic barrier rotor owing to the presence of the assisted cages.

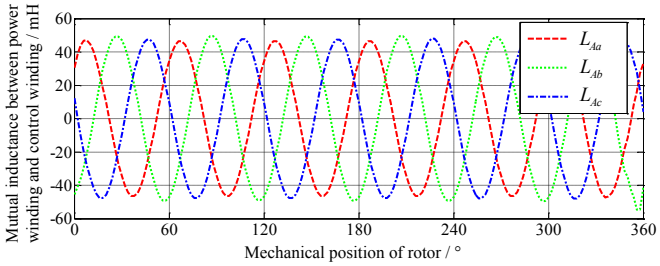

Fig. 13. Mutual inductance between power winding and control winding of an 8/4 BDFG with hybrid rotor.

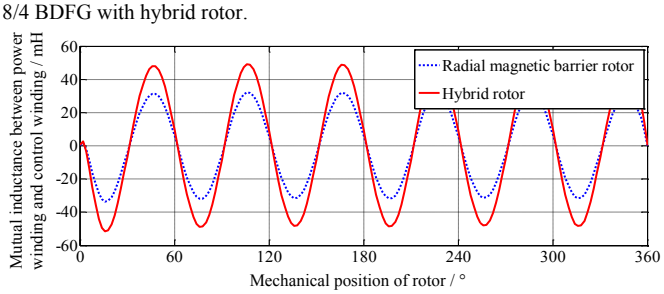

Fig. 14. Comparison of mutual inductance for the considered rotor designs.

This article has been accepted for publication in a future issue of this journal, but has not been fully edited. Content may change prior to final publication. Citation information: DOI 10.1109/TIE.2018.2811379, IEEE Transactions on Industrial Electronics

IV. Experimental Verification

Two prototype BDFGs with the hybrid and radial magnetic barrier rotors have been manufactured to practically verify the design studies and theoretical analysis. The photos of the common stator frame and two rotors appear in Fig. 15, and the relevant design parameters are listed in Table III.

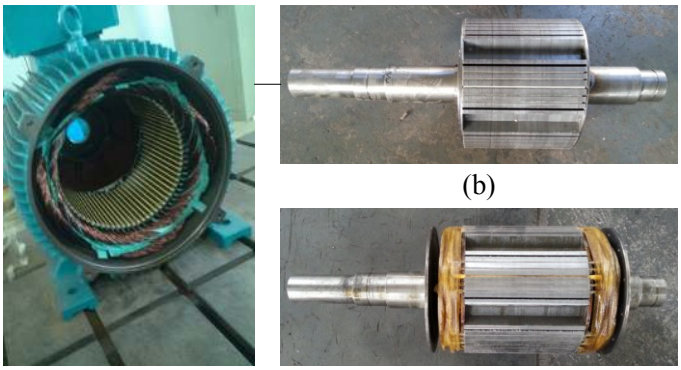

(a) (b) (c)

Fig. 15. The main components of the BDFG prototypes: (a) Stator; (b) Radial magnetic barrier rotor; (c) Hybrid rotor.

TABLE III
SPECIFICATIONS AND DESIGN DETAILS OF THE BDFG PROTOTYPES

Parameter	Symbol	Value
Rated power	P_N	25 kW
Rated voltage of power winding (50 Hz)	U_{Np}	380 V
Rated voltage of control winding (50 Hz)	U_{Nc}	380 V
Rated speed	n_N	1000 r/min
Natural synchronous speed	n_0	500 r/min
Number of stator slots	Z_s	72
Number of power winding pole pairs	p_p	4
Number of control winding pole pairs	p_c	2
Number of power winding coil turns	N_p	6
Number of control winding coil turns	N_c	4
Stator outer diameter	D_{so}	400 mm
Stator inner diameter	D_{si}	285 mm
Air-gap length	g	0.5 mm
Rotor outer diameter	D_{ro}	284 mm
Number of rotor ducts	Z_r	42
Number of magnetic layers	N_{rm}	4
Number of concentric cage groups (hybrid rotor)	N_{rcg}	2
Stack length	L_{ef}	225 mm

A. Measurements

The parameters in Table IV are identified by applying the bridge method and the static test method. The measured mutual inductance values are shown in Fig. 16. Note that the mutual inductance of the hybrid rotor is superior to that of the radial magnetic barrier rotor, which is consistent with the outcomes of the theoretical studies. However, the calculated values are higher than the measurements due to the leakage inductance and slotting effects being ignored in the model.

TABLE IV
PARAMETERS VALUE OF PROTOTYPES

Parameter	Value
Resistance of power winding	0.387 Ω
Resistance of control winding	0.377 Ω
Mutual inductance (radial magnetic barrier rotor)	25 mH
Mutual inductance (hybrid rotor)	38 mH

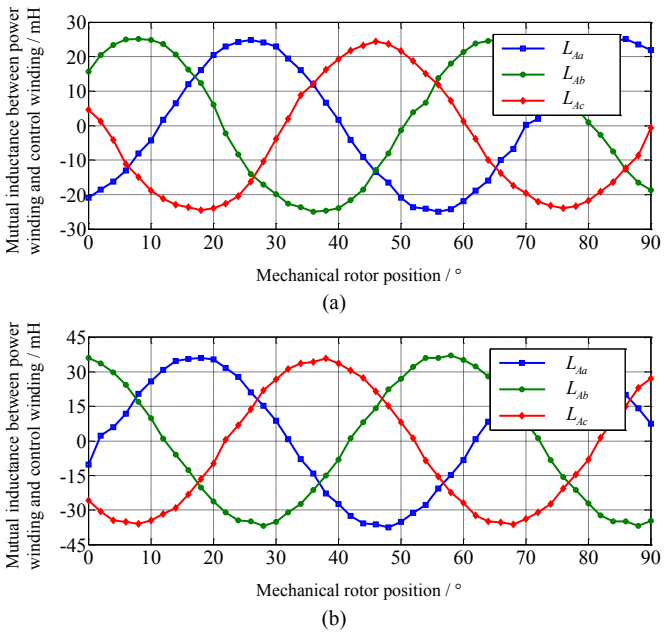

Fig. 16. Experimental results of mutual inductance for: (a) Radial magnetic barrier rotor; (b) Hybrid rotor.

B. BDFG Test Facility

The experimental setup is shown in Fig. 17. When the BDFG is operated in sub-synchronous mode, the power flowing into the control winding should be recognized as the input electrical power together with mechanical, and the efficiency can be estimated as follows:

$$\eta = P_p / (P_c + P_{mech}) \times 100\% = P_p / (P_c + T_L n_r \pi / 30) \times 100\% \quad (27)$$

Conversely, if the BDFG is operated in super-synchronous mode, the power of control winding is considered as output power and the efficiency should be computed as:

$$\eta = (P_p + P_c) / P_{mech} \times 100\% = 30(P_p + P_c) / (T_L n_r \pi) \times 100\% \quad (28)$$

where P_{mech} represents the mechanical (shaft) power.

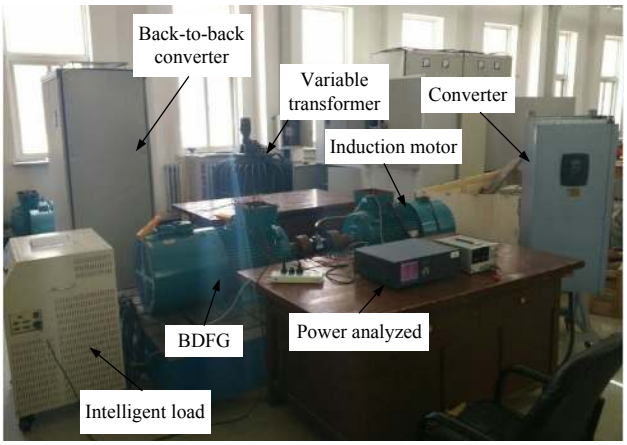

Fig. 17. Experimental platform and apparatus used.

The efficiency of the BDFGs for different operating modes is presented in Fig. 18. As can be seen, the BDFG efficiency with the hybrid rotor is higher than with the magnetic barrier one. The test results show that the magnetic field modulation of the hybrid rotor is better than that of the magnetic barrier

counterpart by virtue of the assisted cages which can clearly enhance the rotor coupling capacity.

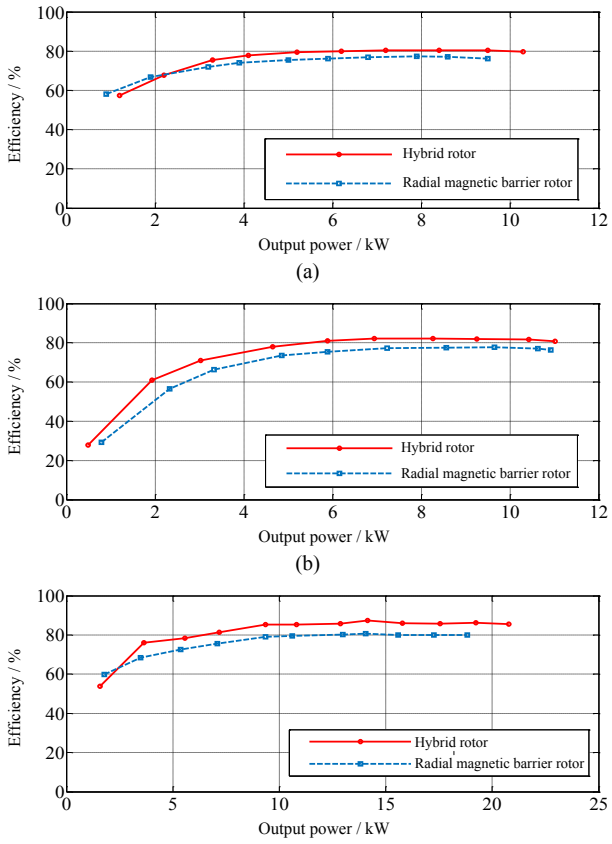

Fig. 18. Efficiency of two BDFG prototypes: (a) Sub-synchronous mode (300 r/min); (b) Super-synchronous mode (800r/min); (c) Rated speed (1000r/min).

The voltage and current waveforms of the BDFG with the hybrid rotor at the rated speed and 14 kW output power are given in Fig. 19. Virtually sinusoidal variations of the voltage and current of the power winding, as well as the control winding current, can be observed.

V. Conclusion

This paper has presented the thorough design and performance studies of the new cage-assisted magnetic barrier rotor (i.e. hybrid rotor) for the BDFG on the basis of the radial magnetic barrier rotor construction applying the magnetic field modulation theory. The influence of various parameters on the rotor modulating capability is fully considered in the design process. The copper and core losses are estimated for the BDFG with both reluctance and hybrid rotor configurations taking into account the harmonic effects. The mutual inductances, used to assess the rotor coupling abilities, are calculated and compared.

Two BDFG test prototypes with the proposed rotor structures have been designed and fabricated for practical evaluations. The accuracy and effectiveness of the theoretical analysis have been validated by the experimental results produced, which have undoubtedly shown that the magnetic field modulation properties and overall performance of the hybrid rotor are clearly superior to those provided by the radial magnetic barrier counterpart. Furthermore, the efficiency of the BDFG with the hybrid rotor is about 3%~6% higher under the same operating conditions to warrant further investigations.

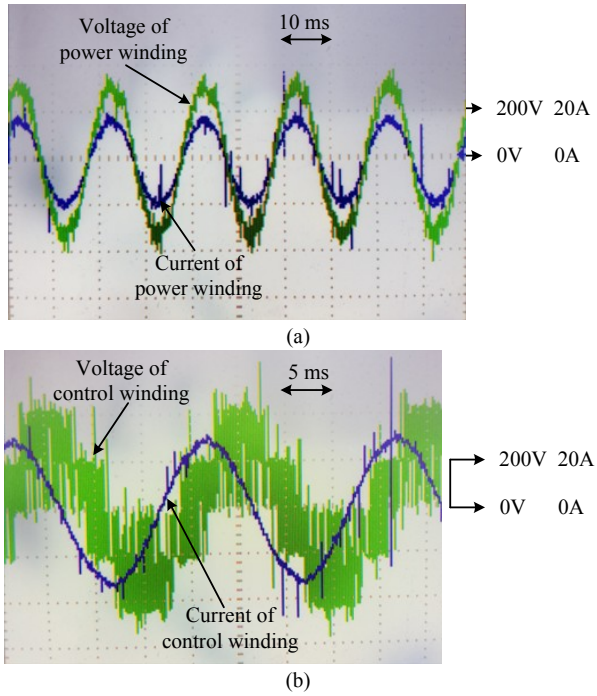

Fig. 19. Recorded voltage and current oscilloscope traces for the BDFG with the hybrid rotor at rated speed: (a) Power winding; (b) Control winding.

References

[1] R. Kumar and S. Das, "MRAS-based speed estimation of grid-connected doubly fed induction machine drive," *IET Power Electron.*, vol. 10, DOI 10.1049/iet-pel.2016.0768, no. 7, pp. 726–737, July 2017.

[2] T. Feehally and J. M. Apsley, "The Doubly Fed Induction Machine as an Aero Generator," *IEEE Trans. Ind. Appl.*, vol. 51, DOI 10.1109/TIA.2015.2413957, no. 4, pp. 3462–3471, July/Aug. 2015.

[3] V. S. S. Kumar and D. Thukaram, "Accurate Steady-State Representation of a Doubly Fed Induction Machine," *IEEE Trans. Power Electron.*, vol. 30, DOI 10.1109/TPEL.2015.2425140, no. 10, pp. 5370–5375, Oct. 2015.

[4] P. Han, M. Cheng and Z. Chen, "Single-Electrical-Port Control of Cascaded Doubly-Fed Induction Machine for EV/HEV Applications," *IEEE Trans. Power Electron.*, vol. 32, DOI 10.1109/TPEL.2016.2623247, no. 9, pp. 7233–7243, Sept. 2017.

[5] R. A. McMahon, P. C. Roberts, X. Wang and P. J. Tavner, "Performance of BDFM as generator and motor," *IEE Proc. Electr. Power Appl.*, vol. 153, DOI 10.1049/ip-epa:20050289, no. 2, pp. 289–299, Mar. 2006.

[6] H. Gorginpour, H. Oraee and R. A. McMahon, "A Novel Modeling Approach for Design Studies of Brushless Doubly Fed Induction Generator Based on Magnetic Equivalent Circuit," *IEEE Trans. Energy Convers.*, vol. 28, DOI 10.1109/TEC.2013.2278486, no. 4, pp. 902–912, Dec. 2013.

[7] S. Ademi, M. G. Jovanovic and M. Hasan, "Control of Brushless Doubly-Fed Reluctance Generators for Wind Energy Conversion Systems," *IEEE Trans. Energy Convers.*, vol. 30, DOI 10.1109/TEC.2014.2385472, no. 2, pp. 596–604, June 2015.

[8] H. Gorginpour, H. Oraee and E. Abdi, "Calculation of Core and Stray Load Losses in Brushless Doubly Fed Induction Generators," *IEEE Trans. Ind. Electron.*, vol. 61, DOI 10.1109/TIE.2013.2279357, no. 7, pp. 3167–3177, July 2014.

[9] E. Abdi, R. A. McMahon, P. Malliband, S. Shao, M. E. Mathekga, P. Tavner, S. Abdi, A.Oraee, T. Long and M. Tatlaw, "Performance Analysis and Testing of a 250 kW Medium-Speed Brushless Doubly-Fed Induction Generator," *IET Renew. Power Gen.*, vol. 7, DOI 10.1049/iet-rpg.2012.0234, no. 6, pp. 631–638, Nov. 2013.

[10] F. Wang, F. Zhang and L. Xu, "Parameter and Performance Comparison of Doubly Fed Brushless Machine with Cage and Reluctance Rotors,"

IEEE Trans. Ind. Appl., vol. 38, DOI 10.1109/TIA.2002.802917, no. 5, pp. 1237–1243, Sept./Oct. 2002.

[11] F. Barati, S. Shao, E. Abdi, H. Oraee and R. A. McMahon, "Generalized Vector Model for the Brushless Doubly-Fed Machine With a Nested-Loop Rotor," *IEEE Trans. Ind. Electron.*, vol. 58, DOI 10.1109/TIE.2010.2064279, no. 6, pp. 2313–2321, June 2011.

[12] T. D. Strous, X. Wang, H. Polinder and J. A. Bram Ferreira, "Brushless Doubly Fed Induction Machines: Magnetic Field Analysis," *IEEE Trans. Magn.*, no. 8108310, Nov. 2016.

[13] H. Gorginpour, B. Jandaghi and H. Oraee, "A Novel Rotor Configuration for Brushless Doubly-Fed Induction Generators," *IET Electr. Power Appl.*, vol. 7, DOI 10.1049/iet-epa.2012.0194, no. 2, pp. 106–115, Feb. 2013.

[14] S. Abdi, E. Abdi, A. Oraee and R. A. McMahon, "Optimization of Magnetic Circuit for Brushless Doubly Fed Machines," *IEEE Trans. Energy Convers.*, vol. 30, DOI 10.1109/TEC.2015.2468063, no. 4, pp. 1611–1620, Dec. 2015.

[15] H. Gorginpour, H. Oraee and R. McMahon, "Electromagnetic-Thermal Design Optimization of the Brushless Doubly Fed Induction Generator," *IEEE Trans. Ind. Electron.*, vol. 61, DOI 10.1109/TIE.2013.2267705, no. 4, pp. 1710–1721, Apr. 2014.

[16] S. Khaliq, S. Atiq, T. A. Lipo and B. Kwon, "Rotor Pole Optimization of Novel Axial-Flux Brushless Doubly Fed Reluctance Machine for Torque Enhancement," *IEEE Trans. Magn.*, no. 8106204, July 2016.

[17] D. G. Dorrell, A. M. Knight, W. K. Song and R. E. Betz, "Saturation and Ducting Effects in a Brushless Doubly-Fed Reluctance Machine," *IEEE Trans. Magn.*, vol. 49, DOI 10.1109/TMAG.2013.2251458, no. 7, pp. 3933–3936, July 2013.

[18] A. M. Knight, R. E. Betz and D. G. Dorrell, "Design and Analysis of Brushless Doubly Fed Reluctance Machines," *IEEE Trans. Ind. Appl.*, vol. 49, DOI 10.1109/TIA.2012.2229451, no. 1, pp. 50–58, Jan./Feb. 2013.

[19] F. Zhang, S. Yu, H. Wang, Y. Wang and D. Wang, "Overview of Research and Development Status of Brushless Doubly-Fed Machine System," *Chinese J. Electr. Eng.*, vol. 2, DOI 10.23919/CJEE.2016.7933122, no. 2, pp. 1–13, Dec. 2016.

[20] F. Blazquez, C. Veganzones, D. Ramirez and C. Platero, "Characterization of the Rotor Magnetic Field in a Brushless Doubly-Fed Induction Machine," *IEEE Trans. Energy Convers.*, vol. 24, DOI 10.1109/TEC.2009.2025345, no. 3, pp. 599–607, Sept. 2009.

[21] D. G. Dorrell, A. M. Knight and R. E. Betz, "Issues with the Design of Brushless Doubly-Fed Reluctance Machines: Unbalance Magnetic pull, Skew and Iron Losses," in *Proc. IEEE IEMDC*, DOI 10.1109/IEMDC.2011.5994890, pp. 663–668, May 2011.

[22] T. A. Lipo, *Analysis of Synchronous Machines*, 2nd ed., Boca Raton, FL, USA: CRC Press, ch. 1, pp. 1-76, 2012.

[23] M. Cheng, P. Han and W. Hua, "General Airgap Field Modulation Theory for Electrical Machines," *IEEE Trans. Ind. Electron.*, vol. 64, DOI 10.1109/TIE.2017.2682792, no. 8, pp. 6063–6074, Aug. 2017.

[24] S. Zhu, M. Cheng, J. Dong and J. Du, "Core Loss Analysis and Calculation of Stator Permanent-Magnet Machine Considering DC-Biased Magnetic Induction," *IEEE Trans. Ind. Electron.*, vol. 61, DOI 10.1109/TIE.2014.2300062, no. 10, pp. 5203–5212, Oct. 2014.

[25] J. Zhu and V. S. Ramsden, "Improved formulations for rotational core losses in rotating electrical machines," *IEEE Trans. Magn.,* vol. 34, DOI 10.1109/20.703861, no. 4, pp. 2234–2242, July 1998.

[26] S. Yu, F. Zhang and H. Wang, "Parameter calculation and analysis of a novel wind power generator," *IEEE Trans. Magn.*, vol. 53, DOI 10.1109/TMAG.2017.2697999, no.11, Nov. 2017, Art. no. 8205607.

Fengge Zhang (M'17) received the B.E.E., M.S., and Ph.D. degrees from the Shenyang University of Technology, Shenyang, China, in 1984, 1990, and 2000, respectively, all in electrical engineering.

Since 1984, he has been with the School of Electrical Engineering, Shenyang University of Technology, where he is currently a Professor. From October 2001 to July 2002, he was a visiting scholar at Esslingen University of Applied Sciences, Esslingen, Germany. He has published numerous journal and conference papers on electrical machines and control systems. His research and teaching interests include electro-magnetic theory, dynamic simulation, magnetic field analysis, optimized design, computer control technology of electrical machines, and wind power generating systems.

Professor Zhang received six paper awards from Liaoning Province and four research awards from the National Machine Industry Ministry, Liaoning Province and Shenyang City, for his outstanding research accomplishments.

Siyang Yu received his B.S. degree in Electrical Engineering from Shenyang University of Technology, Shenyang, China, in 2011. He received the M.S. degrees from both Kyungsung University, Busan, Korea, and Shenyang University of Technology, Shenyang, China, in 2014.

He is currently working toward the Ph.D. degree in Electrical Engineering at Shenyang University of Technology, Shenyang, China. His current research interests include special machine design, electric machine control, and wind power generation.

Yutao Wang received his B.S. degree from the Shenyang University of Technology, Shenyang, China, in 2016. He is currently working toward the M.S. degree at Shenyang University of Technology, Shenyang, China.

His main research interests and activities are in the areas of dynamic modelling, simulations and special machine electro-magnetic design as well as wind power generation.

Shi Jin (M'17) received the B.E., M.S., and Ph.D. degrees from the Shenyang University of Technology, Shenyang, China, in 2004, 2007, and 2011, respectively, all in electrical engineering.

Since 2011, she has been with the School of Electrical Engineering at Shenyang University of Technology. She has published more than 40 journal and conference papers. Her research and teaching interests include power electronics converters, electrical machines and their control systems, and wind power generation.

Dr. Jin has received financial support from the National Natural Science Foundation of China. She was selected for the Baiqianwan Talents Project of Liaoning Province in 2013.

Milutin G. Jovanović (M'99–SM'05) received the Dipl. Eng and M.E.E. degrees from the University of Belgrade, Serbia, in 1987 and 1991, respectively, and the Ph.D. degree from the University of Newcastle, Australia, in 1997, all in electrical power engineering.

He is currently an Associate Professor with the Faculty of Engineering and Environment at Northumbria University Newcastle, Newcastle upon Tyne, United Kingdom. He has published more than 150 journal and conference papers including many book chapters and filed patents. His major interests and activities are in the areas of synchronous reluctance machine drives, power electronics control and applications of doubly-fed motors and/or generators, and wind energy conversion systems.